sciendo

Polish Journal of Chemical Technology, 25, 3, 71—78, 10.2478/pjct-2023-0027

CFD-DEM simulation of raceway size and mechanical characteristics of industrial scale blast furnace

Yuzhen Gao[1], Choon Kit Chan[2,*]

[1]School of Mathematics and Statistics, Huangshan University, Huangshan 245041, China
[2]Faculty of Engineering and Quantity Surveying, INTI International University, 71800, Nilai, Negeri Sembilan, Malaysia
[*]*Corresponding authors: e-mail:* Choonkit.chan@newinti.edu.my

The raceway plays a crucial role in ensuring the stable functioning of the ironmaking blast furnace. It is the key site where the chemical reaction of coke combustion takes place, providing the necessary heat and reducing gas for the upper iron ore reduction process. Consequently, the size of the raceway serves as an essential indicator of the blast furnace's operational condition. In this study, a mathematical model for the raceway of an industrial-scale blast furnace was established. Extensive innovation investigations were conducted to explore the characteristics pertaining to the raceway's size. The simulation outcomes demonstrate that both the particle size and the inlet velocity exert significant influences on the raceway dimensions. Specifically, the height of the raceway is predominantly affected by the particle size, whereas the inlet velocity predominantly influences the depth of the raceway.

Keywords: raceway, CFD-DEM, numerical simulation, blast furnace

INTRODUCTION

Blast furnace is the main equipment for ironmaking. Iron ore and coke are loaded in layers in the furnace[1], and hot air is blown in from the lower tuyere to form the raceway[2]. In the raceway, the air and coke undergo intense momentum exchange and combustion reaction[3], which affects the smoothness of gas-solid flow in the furnace[4]. The shape of the raceway cavity is closely related to the blast furnace efficiency as well because the deeper cavity will make the flue gas better distributed in the furnace[5]. Therefore, a comprehensive study on the raceway size characteristics is of great significance for further understanding the operation of blast furnace and safety production.

The study of blast furnace raceway has been widely carried out in the past few decades. The research methods of raceway can be divided into three categories: measurement method, experimental method, and numerical simulation method.

The measurement method is to measure the size, temperature, and pressure of the raceway by using various measuring instruments or special technologies. Zhang[6] used digital image processing technology to measure and study the temperature distribution of the raceway. Li[7] proposed a method to predict raceway depth using a learning model for blast furnace temperature data. However, due to the high-temperature and high-pressure environment inside the blast furnace during production, it is difficult to detect the situation of raceway exactly. The data obtained by the direct measurement method is limited.

The experimental method is to study the characteristics of the raceway by establishing a physical experimental model. In order to observe the formation and development of the raceway clearly, the quasi-two-dimensional model made of transparent materials is generally used as the experimental container. Hatano[4] conducted a cold state experiment to study the formation of the raceway and measured the depth of the raceway. Burgess[8] conducted thermal state experiments to study the combustion characteristics in the raceway. The work mainly studied the effects of bed filler (such as coke quality), pulverized coal, and other new fuel injections on the shape and size of the raceway and the gas-solid flow characteristics in the furnace. Rajneesh[9] studied the effect of friction on the formation process of the packed bed cavity by experimental method. The result shows that friction has a significant effect on the prediction of cavity size. With the decrease of the internal friction angle between particles, the size of the cavity decreases. The friction angle between the wall and the particles has the opposite trend. Moreover, Rajneesh[10] studied the influence of gas velocity on the change of raceway size in the presence of friction through two-dimensional experiments. Two prediction formulas of raceway size for increasing and decreasing gas velocity are developed, which can effectively predict the hysteresis of the raceway in the cold model. Considering the inhomogeneity of coke particle size in the actual blast furnace, Sastry[11] mixed materials with different particle sizes and carried out two-dimensional experiments in cold state to study the formation and fragmentation of raceway. The results show that there is no significant difference between the mixed particle size system and the uniform particle size system. In addition, compared with the glass system, the expansion of the plexiglass container used in the current work reduces the reproducibility and accuracy of the results.

With the development of blast furnace coal injection technology and oxygen enriched combustion technology, the reaction of raceway becomes more and more complex. The experimental method is limited by the size and operating conditions, and it is difficult to carry out hot combustion experiments, which is more and more difficult to adapt to the study of raceway characteristics. Numerical simulation is an alternative method to fully reveal the gas-solid flow in the raceway. DEM can track the movement of each particle and can obtain detailed information about particle movement and fluid flow in the gas-solid movement field, which is helpful to deeply reveal the mechanism of gas-solid flow in the high-temperature furnace. Nowadays, more and more scholars study the raceway through the numerical simulation method.

E[12] carried out the research of granular reaction flow by CFD-DEM, revealing the dynamic evolution and internal thermochemical behavior of the blast furnace raceway. The method considers the change of particle

diameter caused by coke combustion, and can better evaluate the characteristic phenomenon around the raceway. Wei[13] discussed the influence of particle shape on the shape and pressure drop of blast furnace raceway through experiments and simulations, and improved the prediction correlation of raceway size. The results show that the closer the particle aspect ratio is to 1, the larger the raceway size is. Small resistance and contact force are the main reasons for spherical particles to form large raceways.

Based on FRM and WPM methods, Li[14] developed the particle attrition-breakage model for CFD-DEM simulation and predicted the wear and breakage of coke in industrial-scale raceway. According to the results, the raceway is divided into four regions, and it is pointed out that the attrition zone in the lower part of the cavity is the main place of wear and breakage.

Wang[15] developed a thermochemical sub-model based on CFD-DEM on the MFIX platform, and used the shrinking core model to consider the combustion reaction of coke, which was well verified with the experimental results. The simulation results based on this model show that the increase in inlet velocity will significantly increase the cavity depth of the raceway. Lower inlet velocity, higher bed temperature, and higher oxygen mass fraction can increase CO production and improve blast furnace performance. On this basis, Xu[16] further added the coarse-grained method and the smoothing method to the CFD-DEM, and further optimized the DEM model from the capture and calculation cost of the raceway morphology. The results show that the coarse-grained method reduces the calculation cost by 78.14%, and the smoothing method is more reliable to capture the raceway morphology.

So far, although some studies on the raceway have been carried out, most of them are only on the laboratory scale and the raceway size is only involved at the edge of the main research. There are few special studies on the size characteristics of blast furnace raceway at an industrial scale. Under the industrial scale, the size of coke and the inlet velocity will make the stress of coke in the furnace different. Therefore, it is indispensable to carry out special research on the raceway size on an industrial scale.

The purpose of this paper is to carry out the raceway simulation according to the industrial-scale blast furnace to obtain the size characteristic. The classic CFD-DEM mathematical model is used to investigate the size change of the raceway during its development and formation. Then the distribution of furnace internal force chain under the stable state of the raceway is studied. Finally, by studying the two variables of particle size and inlet velocity, the size variation characteristic of the raceway is obtained.

GOVERNING EQUATION

In CFD-DEM, gas phase is regarded as a continuous phase, governed by Navier-Stokes equations, solid phase tracks each particle separately according to Newton's second law. The collision between particles is solved by soft-sphere approach[17, 18]. Momentum transfer between gas phase and particles is considered according to Gidaspow drag model[19]. The model is briefly introduced here, more details can be found in the MFIX documentation[20, 21].

Gas-phase

Without considering phase transitions and chemical reactions, the mass and momentum conservation equation for gas phase is given by

$$\frac{\partial(\varepsilon_g\rho_g)}{\partial t}+\nabla\cdot(\varepsilon_g\rho_g\boldsymbol{u}_g)=0 \tag{1}$$

$$\frac{\partial}{\partial t}(\varepsilon_g\rho_g\boldsymbol{u}_g)+\nabla\cdot(\varepsilon_g\rho_g\boldsymbol{u}_g\boldsymbol{u}_g)=\nabla\cdot\overline{\boldsymbol{S}_g}+\varepsilon_g\rho_g\boldsymbol{g}-\sum_{m=1}^{M}\boldsymbol{I}_{gm} \tag{2}$$

where ε_g, ρ_g, $\boldsymbol{u}_g$, are the volume fraction, thermodynamic density, average velocity of the gas phase, respectively. I_{gm} is the momentum exchange between the gas and solid phase. $\overline{\boldsymbol{S}_g}$ is the gas phase stress tensor given by

$$\overline{\boldsymbol{S}_g}=-P_g\bar{I}+\overline{\tau_g} \tag{3}$$

$$\overline{\tau_g}=2\mu_g\overline{\boldsymbol{D}_g}+\lambda_g\nabla\cdot tr(\overline{\boldsymbol{D}_g})\bar{I} \tag{4}$$

$$\overline{\boldsymbol{D}_g}=\frac{1}{2}[\nabla\boldsymbol{v}_g+(\nabla\boldsymbol{v}_g)^T] \tag{5}$$

where P_g is the pressure of gas phase. $\overline{\tau_g}$ is the shear stress tensor, $\overline{\boldsymbol{D}_g}$ is the strain rate tensor, $\boldsymbol{\mu}_g$ is the viscosity coefficient, $\boldsymbol{\lambda}_g$ is the second coefficients of viscosity.

The compressible gas follows the equation of state of ideal gases:

$$\rho_g=\frac{P_gM_w}{RT_g} \tag{6}$$

where M_W is the gas molecular weight, T_g is the absolute temperature, and R is the ideal gas constant.

Solid-phase

The position, linear velocity, and angular velocity of spherical particles are obtained according to Newton's second law, and the governing equation is as follows:

$$\frac{d\boldsymbol{X}}{dt}=\boldsymbol{V} \tag{7}$$

$$m\frac{d\boldsymbol{V}}{dt}=mg+\boldsymbol{F}_d+\boldsymbol{F}_c \tag{8}$$

$$I\frac{d\boldsymbol{\omega}}{dt}=T \tag{9}$$

where m and I are particle mass and particle moment of inertia, g is the acceleration due to gravity, $\boldsymbol{F}_d$ is the total drag force (including pressure and viscous) on the particle, $\boldsymbol{F}_c$ is the sum of contact force resulting from other particles, T is the total torques on the particle.

The description of the contact force between particles is based on the spring–dashpot system in the soft-sphere approach, which has unique advantages in dealing with dense phase and multi-particle contact. For two particles i and j, the normal and tangential components ($\boldsymbol{F}_{nij}$ and $\boldsymbol{F}_{nij}$) of the contact force $\boldsymbol{F}_{ij}$, are decomposed into the spring (conservative) force $\boldsymbol{F}_{ij}^S$ and the dashpot (dissipative) force $\boldsymbol{F}_{ij}^D$ as[22]:

$$\boldsymbol{F}_{nij}=\boldsymbol{F}_{nij}^S+\boldsymbol{F}_{nij}^D=(-k_n\delta_n-\eta_nu_{nij})\boldsymbol{n}_{ij} \tag{10}$$

$$\boldsymbol{F}_{tij}=\boldsymbol{F}_{tij}^S+\boldsymbol{F}_{tij}^D=(-k_t\delta_t-\eta_tu_{tij})\boldsymbol{t}_{ij} \tag{11}$$

where n and t denote the normal and tangential directions, respectively. k and η are the coefficients of spring stiffness and dashpot damping. $\boldsymbol{n}_{ij}$ and $\boldsymbol{t}_{ij}$ are the normal and tangential of unit vector along the line of contact pointing from particle i to particle j, δ_n is the overlap in the normal direction, δ_t is the tangential displacement.

The total contact force and torque acting on particle i is calculated by

$$\boldsymbol{F}_c^i = \sum_{\substack{j=1 \\ j\neq i}}^{N} \left(\boldsymbol{F}_{ij}^S + \boldsymbol{F}_{ij}^D\right) \tag{12}$$

$$\boldsymbol{T}^i = \sum_{\substack{j=1 \\ j\neq i}}^{N} \left(\boldsymbol{L}^i n_{ij} \times \boldsymbol{F}_{tij}\right) \tag{13}$$

where L^i the distance of the contact point from the center of particle i.

Gas-solid coupling

In this study, for gas-solid force, the gas pressure gradient and the drag force caused by the velocity difference between phases are taken into accounted. The $\boldsymbol{F}_d$ expression of the force between the gas phase and the solid phase is:

$$\boldsymbol{F}_d = -\nabla P_g V_p + \frac{\beta^k V_p}{\varepsilon_s}\left(\boldsymbol{u}_g - \boldsymbol{u}_s\right) \tag{14}$$

where P_g, $\boldsymbol{u}_g$ are the gas-phase mean pressure and velocity, $\boldsymbol{u}_s$ the particle velocity, $V_p = \frac{\pi d_p^3}{6}$ the particle volume, k is the number of computational cell where particle located, β is the inter-phase momentum exchange coefficient, it is determined by the widely used Gidaspow drag model[19], the accuracy of the model in predicting gas-solid flow patterns has been verified many times[23–25]. The expression for β is as follows:

$$\beta = \begin{cases} 150\dfrac{(1-\varepsilon_g)^2\mu_g}{\varepsilon_g d_p^2} + 1.75\dfrac{(1-\varepsilon_g)\rho_g\left|\boldsymbol{u}_g - \boldsymbol{u}_s\right|}{d_p} & \varepsilon_g \le 0.8 \\ \dfrac{3}{4}\dfrac{\varepsilon_g(1-\varepsilon_g)\rho_g\left|\boldsymbol{u}_g - \boldsymbol{u}_s\right|}{d_p} C_D \varepsilon_g^{-2.65} & \varepsilon_g > 0.8 \end{cases} \tag{15}$$

$$C_D = \begin{cases} 24\dfrac{(1 + 0.15\, Re_g^{0.687})}{Re_g} & Re_g \le 1000 \\ 0.44 & Re_g > 1000 \end{cases} \tag{16}$$

$$Re_g = \frac{\rho_g \varepsilon_g \left|u_g - u_s\right| d_p}{\mu_g} \tag{17}$$

where C_D is the drag coefficient for a single particle. Re_g and d_p are the particle Reynolds number and particle diameter, respectively.

The gas-solid momentum transfer term can be expressed as I_{gs}, at x_k, that enters the gas–phase momentum conservation equation (2) is computed as:

$$\boldsymbol{I}_{gs} = \frac{1}{V_k}\sum_{i=1}^{N} \boldsymbol{F}_d^{i\in k} K\left(\boldsymbol{x}^i, \boldsymbol{x}_k\right) \tag{18}$$

where $K(\boldsymbol{x}^i, \boldsymbol{x}_k)$ is a generic kernel with compact support and determines the influence of the particle force at $\boldsymbol{x}^i$ on a grid node located at $\boldsymbol{x}_k$, and V_k is the geometric volume of the k^{th} grid cell.

SIMULATION CONDITIONS

Based on the size of the industrial blast furnace provided by Li[14], a geometric model is established for numerical simulation to study the formation process and size characteristics of the raceway. The geometric model is simplified as a 130 mm thick sheet with a height of 3450 mm and a length of 2500 mm. The tuyere is a cylindrical tube, 130 mm direct, and 400 mm insertion depth. The model structure and main sizes are shown in Fig. 1. In the simulation, a pure granular flow simulation was conducted first, piling up particles to a height of 2250 mm, which was used as the initial state for the simulation. The main simulation parameters are provided in Table 1.

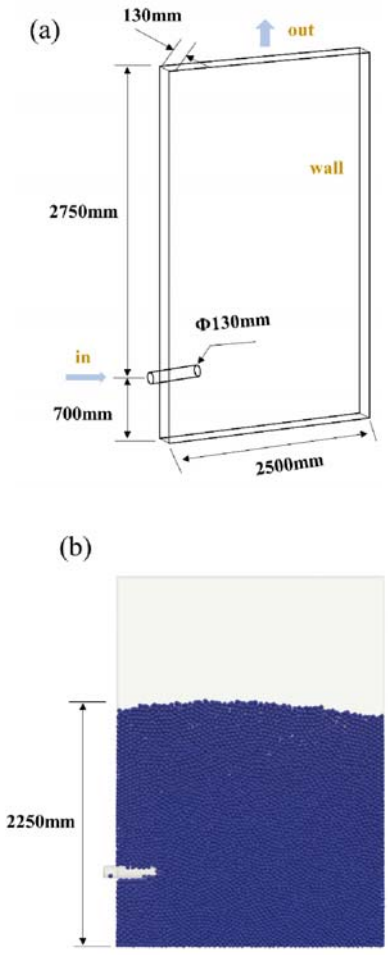

Figure 1. Simulation model and initial state: (a) Geometric structure; (b) Initial packing height of bed

Table 1. Numerical settings and gas–solid parameters used in simulation

Parameter	Value
Particle diameter (mm)	40, 43, 45
Particle density (kg/m^3)	1000
Particle number	17978, 15144, 13274
Particle friction coefficient	0.1
Particle spring constant(N/m)	1000
Restitution coefficients	0.2
Damping coefficient factor	0.5
Computational domain(mm)	2700,3450,130
Number of grid nodes(x,y,z)	57,62,2
Tuyere diameter(mm)	130
Inlet velocity(m/s)	225, 235, 245
Gas viscosity(kg/m^3)	1.8×10^{-5}
Gas molecular weight(g/mol)	29

RESULTS AND DISCUSSION

Model validation

The validation of the CFD-DEM mathematical model is performed based on an experimental study on a lab-scale 2D packed bed in the literature[15]. In the simulation, the packed bed height is set as 3500 mm, and the bed thickness is set as 88 mm. The particle diameter is 40 mm. The parameters of the simulation are shown in Table 2.

Table 2. Simulation parameters used in validation

Parameter	Value
Particle diameter (mm)	40
Particle density (kg/m^3)	1000
Particle number	13325
Particle friction coefficient	0.1
Particle spring constant(N/m)	1000
Restitution coefficients	0.2
Tuyere diameter(mm)	88
Inlet velocity(m/s)	232
Gas viscosity(kg/m^3)	1.8×10^{-5}

Figure 2 shows the size comparison between simulation and experimental results in the steady state raceway. It can be observed that the size of the raceway obtained from the simulation is very close to the experimental results. In Wang's experiment, the raceway exhibited a higher height than depth characteristic. The simulation validates that the heights and depths are similar, primarily influenced by the initial accumulated particle height. The standard deviation for depth is 8.5%, while for height, it is 6.2%. Considering the object's industrial scale, this deviation is acceptable. Therefore, the mathematical model used in this paper is rigorous and effective.

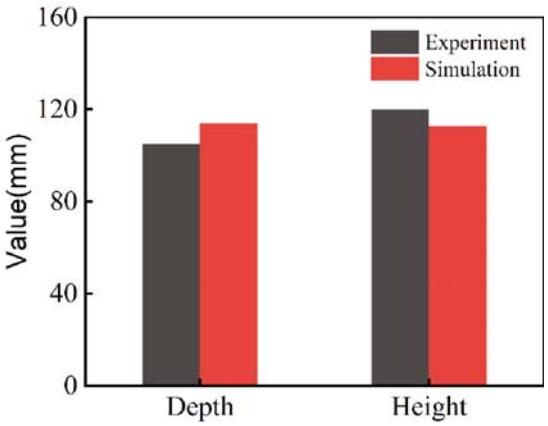

Figure 2. Comparison of raceway size between simulation and experiment

Size characteristics in the formation of raceway

The stable raceway has a relatively stable size which can be measured. For simulation, the particle size and position distribution images under stable conditions are extracted many times, and clear edges are obtained through binary processing. The maximum vertical axis difference and horizontal axis difference of points on the edge line are calculated as the height and depth.

The development and formation process of the raceway are illustrated in Fig. 3. The change in size of the raceway is depicted in Fig. 4. Upon the injection of air flow, particles located near the air vent are blown away, and the opening of the air vent begins to expand gradually, resulting in the formation of a spherical cavity. As shown in Fig. 4, the height and depth of the raceway at this stage are approximately equal. Moreover, as the air flow continues to be injected, the raceway transforms into a narrow and elongated shape, exemplifying a scenario where the depth surpasses the height, as shown in Fig. 3(b). This characteristic can be attributed to the continuous high-speed transverse intake of air, generating a significant transverse impact on the particles. Additionally, Fig. 4 indicates that the horizontal expansion of the raceway occurs most rapidly during this phase. By the 3-second mark, owing to the compact structure of the deadman, the end of the narrow raceway cavity rises and extends in an upward direction, prompting the particles to commence a counterclockwise movement within the raceway. Consequently, the height of the raceway at this point is greater than that in (b). At 4 seconds, the cavity shape has essentially reached its final form, and the increase in height and depth of the raceway area becomes relatively gradual. By the 6-second mark, a relatively stable raceway cavity with ellipsoidal characteristics has been established, and particles continue to move counterclockwise within it. Notably, the strong interaction forces between particles and the fluid led to particle detachment from the inner surface of the raceway, thereby achieving a state of dynamic equilibrium[26].

Distribution of force chain in the raceway

The velocity and collision force distribution of particles in the steady-state raceway are shown in Fig. 5. The particles at the tuyere are directly accelerated by the

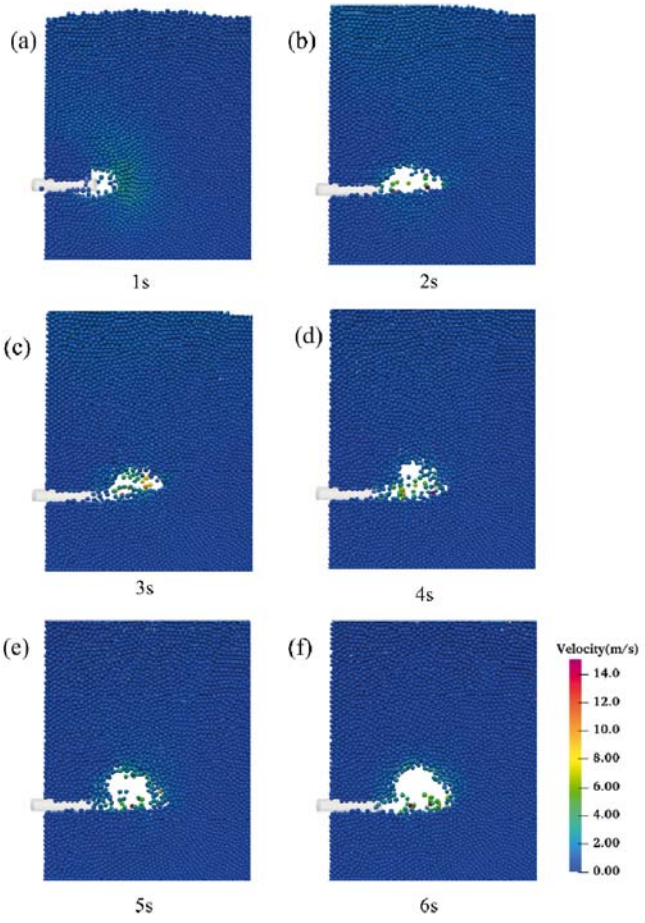

Figure 3. The development and formation process of the raceway

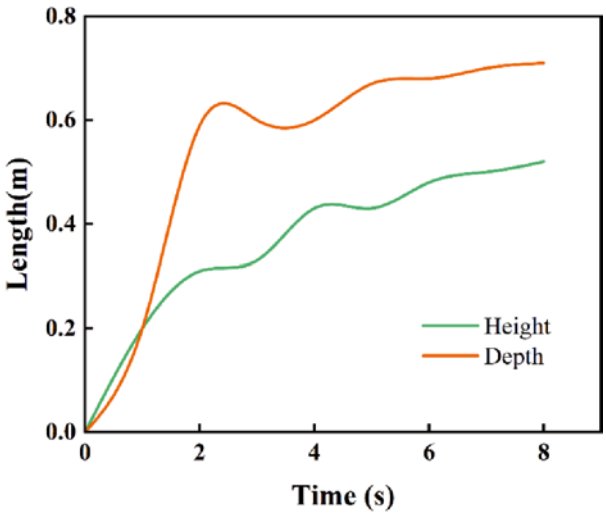

Figure 4. Size change during the raceway formation

airflow, and the linear velocity reaches the maximum at the deepest point of the cavity. This is consistent with Li's research. The maximum kinetic energy also makes the cavity deepest point the most worn and broken area[14]. Fig. 5(b) shows the particle angular velocity distribution. It can be seen that most particles are doing their own rotation in the motion of the raceway. The angular velocity of particles in the lower part of the cavity is the largest, and the range of particles affected by the cyclotron motion is also much larger than that in the cavity. E's research[12, 27] shows that when the drag force exceeds the gravity of particles, the interlocking mechanism between particles will be destroyed. The increase of the rotational kinetic energy of the particles themselves in the raceway is also constantly reconstructing the porous structure of the raceway nearby.

The collision force on the particle is almost consistent with the linear velocity distribution. The force in the lower part of the raceway is large, but in the upper part of the cavity is obviously small. The upper particles are mainly supported by air flow. The collision of particles in the lower part of the cavity has released most of the kinetic energy, and the kinetic energy is small when moving above the cavity.

Fig. 6 shows the force chain distribution in and around the raceway. Fig. 6(a) shows the magnitude non-dimensionalized by the average value, and (b) shows the distance between the particles and is smaller than the diameter since there is a small overlap. We can see the lower part of the raceway and deeper, the deadman, subject to the largest force. Compared with the periphery of the raceway, the upper force of the computational domain is relatively small. In the dynamic state, the static structure of the upper bed layer is disrupted, resulting in a weak pressure distribution above the raceway cavity region[28]. In the deadman, the particles experience compression, resulting in a denser bed layer structure.

Sensitivity analysis on the raceway size

The sensitivity analysis of the size of the raceway is mainly carried out for the two factors of inlet velocity and particle size. Fig. 7 and Fig. 8 show the variation of the raceway size from the inlet velocity and particle size, respectively. For different conditions, the cavity always shows that the depth is greater than the height. The larger the particle size is, the greater the ratio of depth to height is, and the flatter the cavity is. Inlet velocity affects the ratio of depth to height. When the particle size is 40 mm, the ratio of depth to height increases with

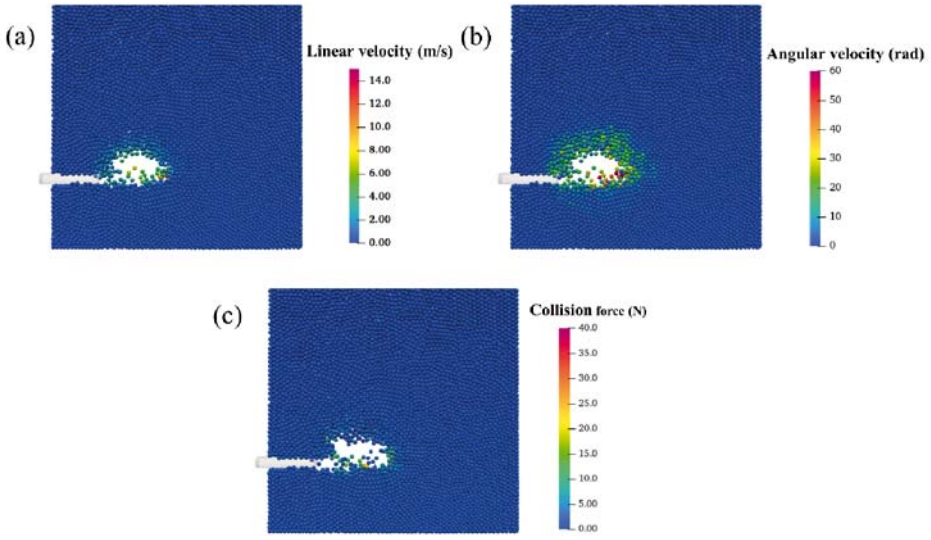

Figure 5. Particle velocity and collision force distribution in the raceway: (a) Linear velocity; (b) Angular velocity; (c) Collision force

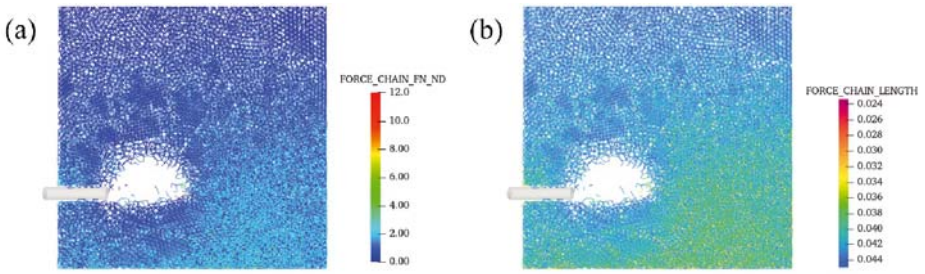

Figure 6. Distribution of force chain nearby the raceway

the increase of inlet velocity. For 43 mm and 45 mm particles, the depth-to-height ratio decreases with the increase of inlet velocity. This is because the structure of the particle layer formed by small particles is not dense enough, and the air flow is easier to enter the depth of the cavity. The particle layer formed by large particles is relatively compact, and the air flow is more moving upward. Particles with small size are more sensitive to the height of the raceway at lower inlet velocity. At 225 m/s velocity, the height of the raceway formed by 40 mm particles is about 1.7 times higher than that of 43 mm and 45 mm. As the inlet velocity increases, the difference in height decreases. The influence of inlet velocity and particle size on the depth of the raceway is relatively small. Under the velocity of 225 m/s, 235 m/s and 245 m/s, the maximum deviation of the raceway depth of different particle sizes is 21.7%, 11.3% and 18.9% respectively.

Figure 9 shows the three-dimensional surface diagram of the influence of inlet velocity and particle size on the raceway size. For height, the smaller the particle size and the larger the inlet velocity, the higher the height of the raceway. In the range of particle size from 45 mm to 40 mm, the influence of particle size on the height of raceway is always large. However, the inlet velocity has a greater impact on the height of the raceway when

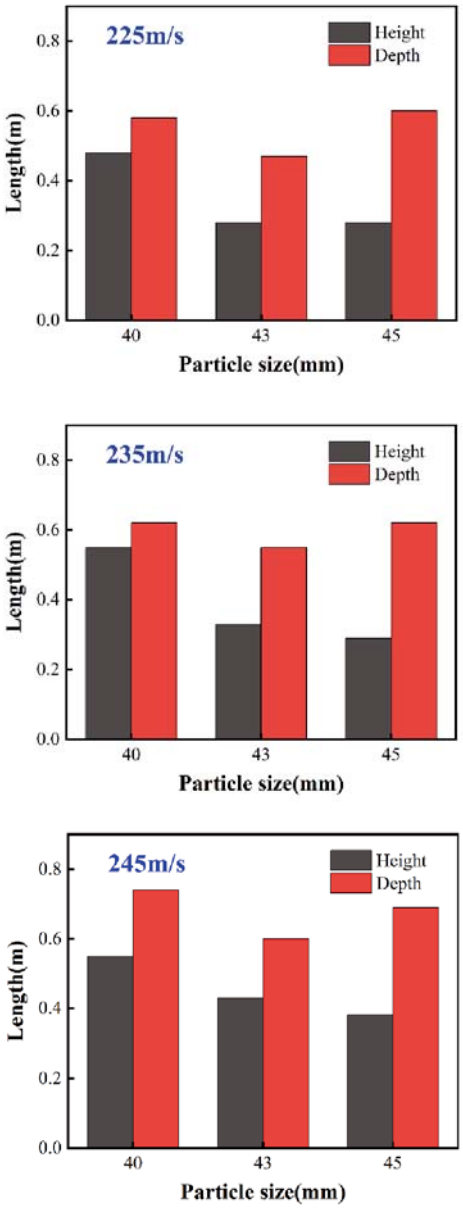

Figure 7. Size of raceway under different inlet velocity: (a) 225 m/s; (b) 235 m/s; (c) 24 5m/s

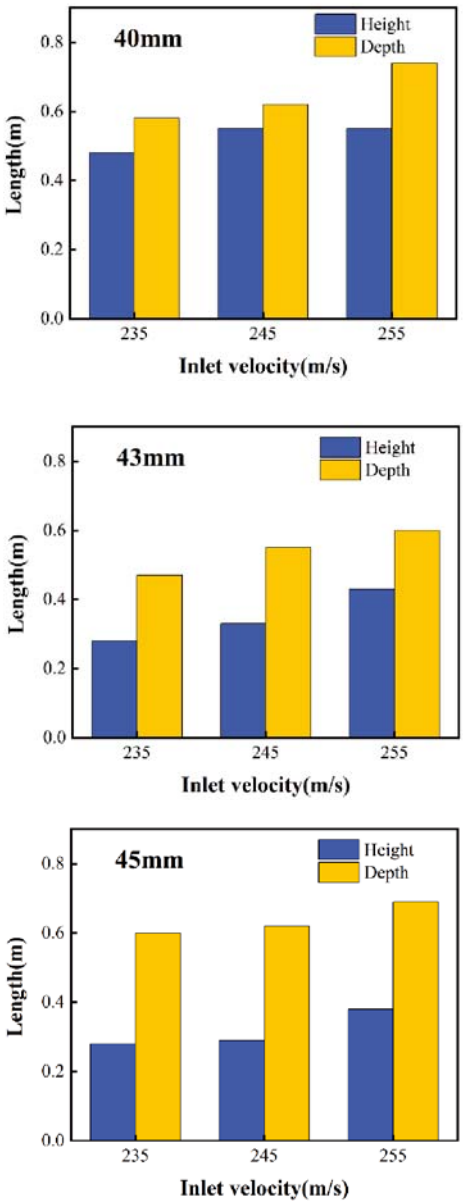

Figure 8. Size of raceway under different particle sizes: (a) 40 mm; (b) 43 mm; (c) 45 mm

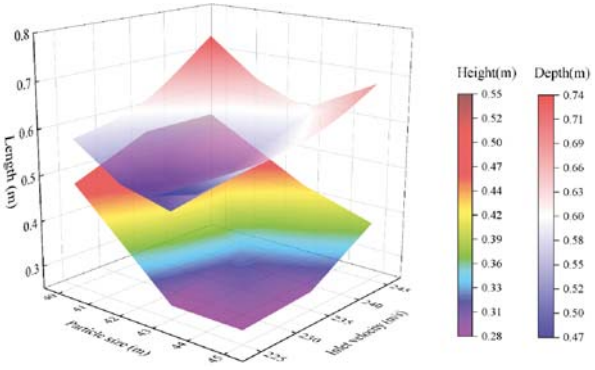

Figure 9. Effect of inlet velocity and particle size on the raceway size

it is from 225 m/s to 235 m/s, and the impact tends to slow down when it is from 235 m/s to 245 m/s. For the depth, the inlet velocity has the strongest impact on the depth. With the increase in velocity, the depth increases significantly. When the particle size is 43 mm, the depth of the raceway is smaller than that of 40 mm and 45 mm.

CONCLUSIONS

The presented work focuses on thoroughly studying the size characteristics and mechanical properties of the industrial-scale blast furnace raceway by means of simulation. The key conclusions from this research are as follows:

1. Formation of the raceway begins with the depth and height values being close to each other, eventually resulting in the creation of an ellipsoidal cavity with significantly greater depth than height.

2. The strength of the force chain is higher at the periphery of the raceway area compared to the upper part. However, the maximum stress area occurs at the depth, particularly at the deadman and lower part of the cavity.

3. Both particle size and inlet velocity exert a significant impact on the size of the raceway. Changes in particle size have a high sensitivity to the height of the raceway, while the inlet velocity directly influences the depth of the raceway.

Moving forward, the future work will involve considering the size characteristics of the industrial-scale blast furnace raceway under thermal conditions. This analysis will involve taking into account factors such as the oxygen content of the inlet gas and bed temperature.

Funding

We would like to acknowledge the financial supports by Key Research Project Fund of Huangshan University (No. 2022xskzd002) and Anhui College Students Innovation and Entrepreneurship Training Fund (202210375107).

LITERATURE CITED

1. Dong, X., Yu, A., Yagi, J.-I. & Zulli, P. (2007). Modelling of multiphase flow in a blast furnace: Recent developments and future work. ISIJ Int., 47, 1553–1570. DOI: 10.2355/isijinternational.47.1553.

2. Hilton, J.E. & Cleary, P.W. (2012). Raceway formation in laterally gas-driven particle beds. *Chem. Eng. Sci*., 80, 306–316. DOI: 10.1016/j.ces.2012.06.044.

3. Mathieson, J.G., Truelove, J.S. & Rogers, H. (2005). Toward an understanding of coal combustion in blast furnace tuyere injection. *Fuel*., 84, 1229–1237. DOI: 10.1016/j.fuel.2004.06.036.

4. Hatano, M., Fukuda, M. & Takeuchi, M. (1976). An experimental study of the formation of raceway using a cold model. Trans. Iron Steel Inst. Jpn., 62, 25–32. DOI: 10.2355/tetsutohagane1955.62.1_25.

5. Straka, R., Bernasowski, M., Klimczyk, A., Stachura, R. & Svyetlichnyy, D. (2020). Prediction of raceway shape in zinc blast furnace under the different blast parameters. Energy., 207. DOI: 10.1016/j.energy.2020.118153.

6. Zhang, S., Wen, L., Bai, C., Chen, D. & Ouyang Q. (2006). The temperature field digitization of radiation images in blast furnace raceway. ISIJ Int., 46, 1410–1415. DOI: 10.2355/isijinternational.46.1410.

7. Li, W., Zhuo, Y., Bao, J. & Shen, Y. (2021). A data-based soft-sensor approach to estimating raceway depth in ironmaking blast furnaces. *Powder Technol*., 390, 529–538. DOI: 10.1016/j.powtec.2021.05.072.

8. Burgess, J.M. (1985). Fuel combustion in the blast furnace raceway zone. Prog. Energy Combust. Sci., 11, 6182. DOI: 10.1016/0360-1285(85)90013-9.

9. Rajneesh, S. & Gupta, G.S. (2003). Importance of frictional forces on the formation of cavity in a packed bed under cross flow of gas. *Powder Technol.,* 134, 72–85. DOI: 10.1016/s0032-5910(03)00136-0.

10. Rajneesh, S., Sarkar, S. & Gupta, G.S. (2004). Prediction of raceway size in blast furnace from two dimensional experimental correlations. ISIJ Int., 44, 1298–1307. DOI: 10.2355/isijinternational.44.1298.

11. Sastry, G.S.S.R.K., Gupta, G.S. & Lahiri, A.K. (2003). Cold model study of raceway under mixed particle conditions. Ironmaking & Steelmaking, 30, 61–65. DOI: 10.1179/030192303225009498.

12. Zhou, D.E.P., Guo, S., Zeng, J., Xu, Q., Guo, L., Hou, Q. & Yu, A. (2022). Particle-scale study of coke combustion in the raceway of an ironmaking blast furnace. *Fuel*., 311. DOI: 10.1016/j.fuel.2021.122490.

13. Wei, G., Zhang, H., An, X., & Hou, Q. (2022). Effect of particle shape on raceway size and pressure drop in a blast furnace: Experimental, numerical and theoretical analyses. *Adv. Powder Technol*., 33. DOI: 10.1016/j.apt.2022.103455.

14. Li, X., Pang, K., Liang, C., Liu, D., Ma, J. & Chen, X. (2023). Particle attrition-breakage model for CFD-DEM simulation based on FRM and WPM: Application in blast furnace raceway. *Powder Technol.,* 414. DOI: 10.1016/j.powtec.2022.118105.

15. Wang, S. & Shen, Y. (2021). CFD-DEM modelling of raceway dynamics and coke combustion in an ironmaking blast furnace. *Fuel*, 302. DOI: 10.1016/j.fuel.2021.121167.

16. Xu, D., Wang, S. & Shen, Y. (2023). An improved CFD--DEM modelling of raceway dynamics and coke combustion in an industrial-scale blast furnace. *Chem. Eng. J.*, 455. DOI: 10.1016/j.cej.2022.140677.

17. Cundall, P.A. & Strack, O.D.L. (1979). A discrete numerical model for granular assemblies. Géotechnique., 29, 47–65. DOI: 10.1680/geot.1979.29.1.47.

18. Tsuji, Y., Kawaguchi, T. & Tanaka, T. (1993). Discrete particle simulation of two-dimensional fluidized bed. *Powder Technol*., 77, 79–87. DOI: 10.1016/0032-5910(93)85010-7.

19. Ding, J. & Gidaspow, D. (1990). A bubbling fluidization model using kinetic theory of granular flow. *AlChE J*., 36, 523–538. DOI: 10.1002/aic.690360404.

20. Garg, R., Galvin, J., Li, T. & Pannala, S. (2012). Documentation of open-source MFIX–DEM software for gas-solids flows. https://mfix.netl.doe.gov/doc/mfix-archive/mfix_current_documentation/dem_doc_2012-1.pdf

21. Garg, R., Galvin, J., Li, T. & Pannala, S. (2012). Open-source MFIX-DEM software for gas–solids flows: Part I—Verification studies. *Powder Technol*., 220, 122–137. DOI: 10.1016/j.powtec.2011.09.019.

22. van der Hoef, M.A., Ye, M., van Sint Annaland, M., Andrews, A.T., Sundaresan, S. & Kuipers, J.A.M. (2006). Multiscale modeling of gas-fluidized beds. Computational Fluid Dynamics. pp. 65–149.

23. Hu, C., Luo, K., Wang, S., Sun, L. & Fan, J. (2019). Influences of operating parameters on the fluidized bed coal gasification process: A coarse-grained CFD-DEM study. *Chem. Eng. Sci*., 195, 693–706. DOI: 10.1016/j.ces.2018.10.015.

24. Ku, X., Jin, H. & Lin, J. (2017). Comparison of gasification performances between raw and torrefied biomasses in an air-blown fluidized-bed gasifier. *Chem. Eng. Sci*., 168, 235–249. DOI: 10.1016/j.ces.2017.04.050.

25. Wang, S., Luo, K. & Fan, J. (2020). CFD-DEM coupled with thermochemical sub-models for biomass gasification: Validation and sensitivity analysis. *Chem. Eng. Sci.*, 217. DOI: 10.1016/j.ces.2020.115550.

26. Hou, Q. & Yu, D.E.A. (2016). Discrete particle modeling of lateral jets into a packed bed and micromechanical analysis of the stability of raceways. *AlChE J*., 62, 4240–4250. DOI: 10.1002/aic.15358.

27. Zhou, D.E.P., Guo, S., Zeng, J., Cui, J., Jiang, Y., Lu, Y., Jiang, Z., Li, Z. & Kuang, S. (2022). Particle shape effect on hydrodynamics and heat transfer in spouted bed: A CFD–DEM study. Particuology., 69, 10–21. DOI: 10.1016/j.partic.2021.11.009.

28. Zhou, D.E.P., Ji, L., Cui, J., Xu, Q., Guo, L. & Yu, A. (2023). Particle-scale modelling of injected hydrogen and coke co-combustion in the raceway of an ironmaking blast furnace. *Fuel*., 336. DOI: 10.1016/j.fuel.2022.126778.